

Article

Polyhedral Phenylacetylenes: The Interplay of Aromaticity and Antiaromaticity in Convex Graphyne Substructures

Daniel Sebastiani ^{1,2,*} and Matt A. Parker ³

¹ Physics Department, Free University Berlin, Arnimallee 14, 14195 Berlin, Germany

² MPI Polymer Research, Ackermannweg 10, 55128 Mainz, Germany

³ Department of Chemistry and Biochemistry, San Diego State University, San Diego, CA 92182, USA

* Author to whom correspondence should be addressed; E-Mail: daniel.sebastiani@fu-berlin.de; Tel.: +49-30-838-53037; Fax: +49-30-838-56046.

Received: 10 November 2009 / Accepted: 27 November 2009 / Published: 11 December 2009

Abstract: We have studied a series of bridged phenylacetylene macrocycles with topologies based on Platonic and Archimedean polyhedra, using density functional calculations to determine both their molecular structure and their electronic response to external magnetic fields (NICS maps). We are able to elucidate the interplay of aromaticity and anti-aromaticity as a function of structural parameters, in particular the symmetry properties of the intramolecular bond connectivities, in these compounds.

Keywords: aromaticity; nucleus independent chemical shifts; density functional theory calculations; phenylacetylene; graphyne

Classification: PACS 31.15.A-, 33.15.Bh, 31.15.E-, 33.25.+k

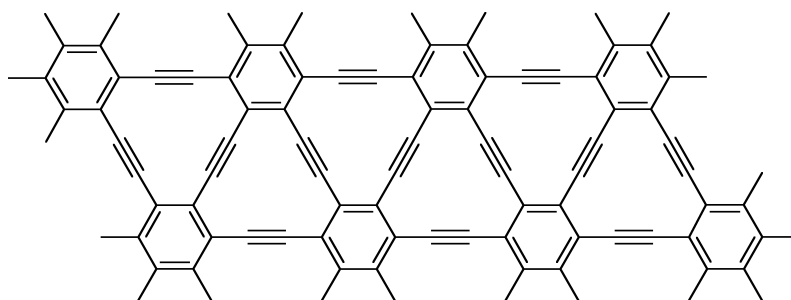
1. Introduction

Graphite is the well-known lowest-energy unsaturated allotrope of carbon, consisting entirely of sp²-hybridized atoms in extended sheets in which benzene is the smallest subunit. This allotrope is topologically analogous to simple hexagonal tiling of the Euclidean plane (zero curvature). Smalley's seminal discovery of C₆₀ opened new vistas of exploration by showing that an allotrope with positively-curved topology was also quite stable, analogous to the symmetrical Archimedean solid A11

(the truncated icosahedron) with 32 faces and 60 vertices, in which a carbon atom is present at each vertex [1, 2]. Further work produced other less positively curved and less symmetrical allotropes such as C_{70} , as well as linearly-extended nanotubes. Additionally, theoretical papers have subsequently described smaller, higher-energy fullerene-like molecules such as C_{20} , C_{36} , and C_{48} [3–6] (the most symmetrical isomer of which is analogous to Archimedean solid A3, the great rhombicuboctahedron, with 48 vertices and Oh symmetry), though no reasonable strategy for their synthesis has been forthcoming [7–11].

Another direction in which theoretical and experimental study of carbon-rich systems has recently proceeded is toward the conceptual expansion of graphite by insertion of sp-hybridized acetylene units between adjacent phenyl rings, giving the structure known as graphyne, shown in Figure 1 [12, 13]. Though the synthesis of graphyne has remained elusive, successively larger fragments have been modeled and synthesized in attempts to predict properties of the bulk material, and these fragments have interesting properties in their own right. In a recent theoretical work on graphyne molecules and oligomers [14], the relationships between aromaticity, HOMO-LUMO-gaps and the molecular connectivities are discussed, using a set of different conjugation pathways.

Figure 1. Molecular structure of graphyne.



In the current work, we combine these two directions of exploration, introducing positive curvature to curl the graphyne sheet upon itself in the same way that C_{60} and the fullerenes represent positive curvature of graphite. We use the Platonic and Archimedean polyhedra as a guide to the simplest and most symmetrical such structures allowed in three-dimensional space, and predict molecular geometries and aromaticities of the resulting molecules using density-functional theory electronic structure calculations [15–19]. In order to examine the inventory of potential convex graphyne substructures guided by the geometry of the aforementioned polyhedra, we transformed each polyhedral vertex into a phenyl ring and each edge into an acetylene unit, according to the data in Table 1.

For the studies undertaken here, we chose the three valid transformations of the Platonic solids (P1, P2, and P4) as well as the two most symmetrical of the Archimedean solids (A1 and A4), shown in Figure 2.

In addition, we examined mono- and bicyclic ring fragments of A1 in order to discover how the aromaticity or anti-aromaticity might vary as a function of the number of pericyclic electron paths around the “great circles” of the spheroidal molecule. The smallest graphyne subfragment “tribenzo” was included for comparative purposes, as was the fullerene C_{60} . The relative sizes of the polyhedral molecules are depicted in Figure 3 (P1 is not shown but is comparable in size to C_{60}).

Table 1. Platonic and Archimedean templates for graphyne macrocycles. For the polyhedra marked with an asterisk*, the sixfold rotational symmetry of the phenyl ring is a poor match for the vertex geometry.

Polyhedron designation (name)	Vertices (C6)	Edges (C2)	Molecular formula
P1 (tetrahedron)	4	6	C36H12
P2 (cube)	8	12	C72H24
P3 (octahedron)	6	12	–*
P4 (dodecahedron)	20	30	C180H60
P5 (icosahedron)	12	30	–*
A1 (cuboctahedron)	12	24	C120H24
A2 (great rhombicosidodecahedron)	120	180	C1080H360
A3 (great rhombicuboctahedron)	48	72	C432H144
A4 (icosidodecahedron)	30	60	C300H60
A5 (small rhombicosidodecahedron)	60	120	–*
A6 (small rhombicuboctahedron)	24	48	–*
A7 (snub cube)	24	60	C264H24
A8 (snub dodecahedron)	60	150	C660H60
A9 (truncated cube)	24	36	C216H72
A10 (truncated dodecahedron)	60	90	C540H180
A11 (truncated icosahedron)	60	90	C540H180
A12 (truncated octahedron)	24	36	C216H72
A13 (truncated tetrahedron)	12	18	C108H36

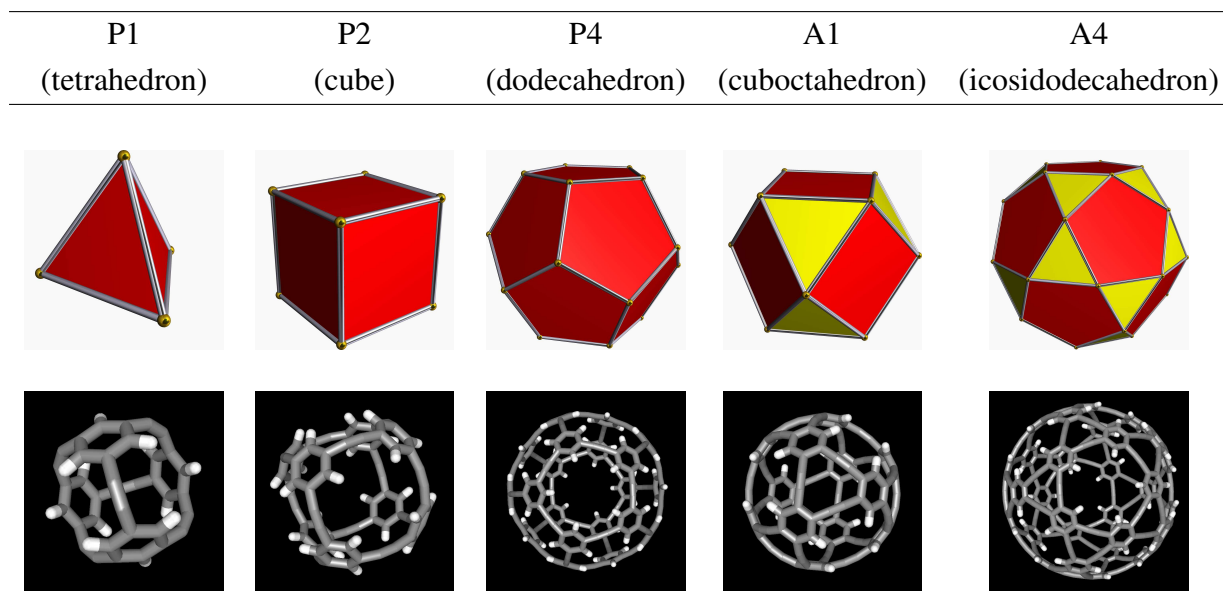
2. Computational Methods

The electronic configuration of our molecules and the graphyne sheet were characterized by means of Nucleus Independent Chemical Shift (NICS) maps, which is a measure of the electronic linear response to an external magnetic field B [19–24]. NICS maps are a generalization of nuclear magnetic shielding tensors as known from NMR spectroscopy, where they quantify the screening of the nuclear spins from the external magnetic field due to ring currents of the electronic orbitals [25–29]. This screening effect is not only defined for the actual nuclear spins, but in all points of space. A large spatial extent of the shielding field indicates a strong aromatic response of the electrons, while a local increase of the external field is a common consequence of an antiaromatic character of the electrons. The electronically induced field is proportional to the externally applied one, so that in practice, the proportionality coefficient is calculated; this factor is dimensionless, because it is the ratio between two magnetic fields. Since its magnitude is typically of the order of 10^{-6} , it is normally given in ppm (parts per million, 10^{-6}).

We compute the effect of such a field using a perturbation theory approach, in which the B-field is considered a small perturbation of the electronic Hamilton operator [17, 18, 30–32]. All calculations were done within Kohn-Sham density functional theory, using the CPMD simulation package [16, 33, 34]. Goedecker-type pseudopotentials were used to describe the interaction of

the valence shell with the nuclei and their core electrons [35, 36]. We have used the BLYP exchange-correlation functional [37, 38] and a plane-wave basis set with a kinetic energy cutoff of 60 Ry for the valence orbitals.

Figure 2. Polyhedral phenylacetylenes paired with their respective polyhedra.



The response of the electronic subsystem to an external magnetic field is a quantum mechanical current density distribution. Via an integration according to the law of Biot-Savart, an (inhomogeneous) induced magnetic field can be derived from the latter, which typically results in a local attenuation of the external field (*i.e.*, a screening or shielding reaction). However, the induced magnetic field may also be locally aligned with the external field, especially in regions with low electronic density, so that the field is increased in amplitude. This effect is called deshielding.

There is a close connection between spatial shielding/deshielding and the characteristics of the electronic configuration [21, 39–42]. Aromatic electron systems induce a large shielded area around themselves, while deshielded regions are a typical signature of an anti-aromatic electronic subsystem [22, 23, 43–45]. Note, however, that in regions of sizeable electronic density, the shielding always dominates; the different signatures are only visible distances of about an Angstroms or more from the covalent bonds.

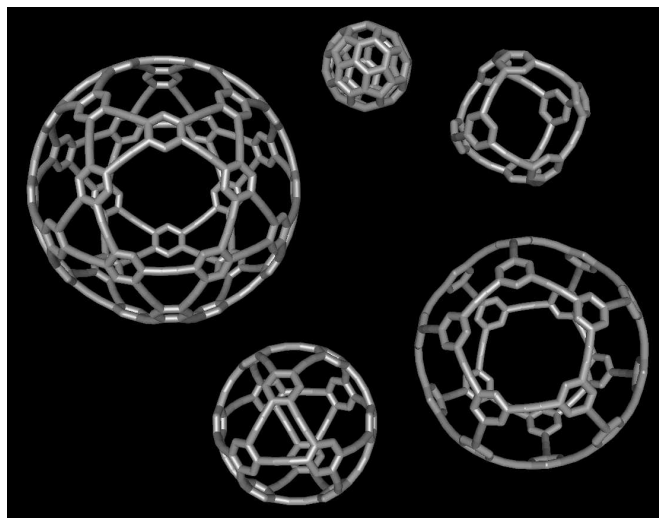
3. Results

3.1. Energies of formation

We have optimized the geometry and the lattice constant of an infinite periodic graphyne slab with a sheet distance of 12 Å, yielding a lattice constant of $a = 6.9708$ Å. In order to check for finite size effects, we have computed the difference of the total energy per carbon with respect to larger unit cells, corresponding to doubling the cell in the two periodic dimensions. Up to a cell of 192 carbon atoms, the

total energy per carbon changed by about 0.22 kcal/mol per carbon, which is very small on the scale of covalent binding energies.

Figure 3. Size comparison of polyhedral phenylacetylenes, with fullerene C₆₀ included for comparison. Clockwise from top: C₆₀, P2, P4, A1, A4.



We have computed the binding energies per carbon atom of the series of polyhedra considered in this work, relative to the energy of a carbon of an infinite graphyne sheet. Since the phenylacetylene molecules contain hydrogen atoms to saturate the structures, we have subtracted the energy of a hydrogen in an isolated oligo-phenylacetylene (C₆₆H₁₈) molecule. This enables us to get mutually comparable values.

Our results are reported in Table 1. It is obvious that the larger structures (A4 and P4) are energetically better than the smaller corresponding cages (A1 and P2/P1), which can be attributed to the weaker curvature in the large molecules. Regarding the smaller molecules (the PA trimer/hexamer/decamer), the apparently counterintuitive energetic ordering can be explained in the same way: The flat trimer has essentially no internal stress, while in the decamer, several bonds are strongly distorted and the hexamer ring is situated in between the other two.

3.2. Link topology

In graphyne, every carbon of a phenyl ring has an acetylene group attached, which connects to a neighboring phenyl. For the isolated molecules in turn, the connectivity is always partially reduced, and some phenyl carbons are saturated with hydrogens. The different connectivity topologies types lead to three-, four-, and five-membered rings (where each member is one phenyl group). These topologies can also be characterized via the relative phenyl positions of the carbons by which a closed loop can be constructed within the molecules. As an example, a three-membered PA ring always consists of phenyl members which are connected via ortho-carbons, while the big hexamer ring has only links on the para positions.

We will use these topologies and the number of triple bonds per molecule and per closed loop as additional characteristics of the various PA oligomers, and we will try to correlate them to the respective magnetic response properties (diatropic or paratropic). In simple conjugated rings, an analogous model exists which correlates the number of conjugated π -bonds to aromaticity. This so-called “ $4 \times n + 2$ ”-rule states that molecules with $4 \times n + 2$ electrons in a conjugated ring system are aromatic (while molecules with $4 \times n$ electrons are antiaromatic).

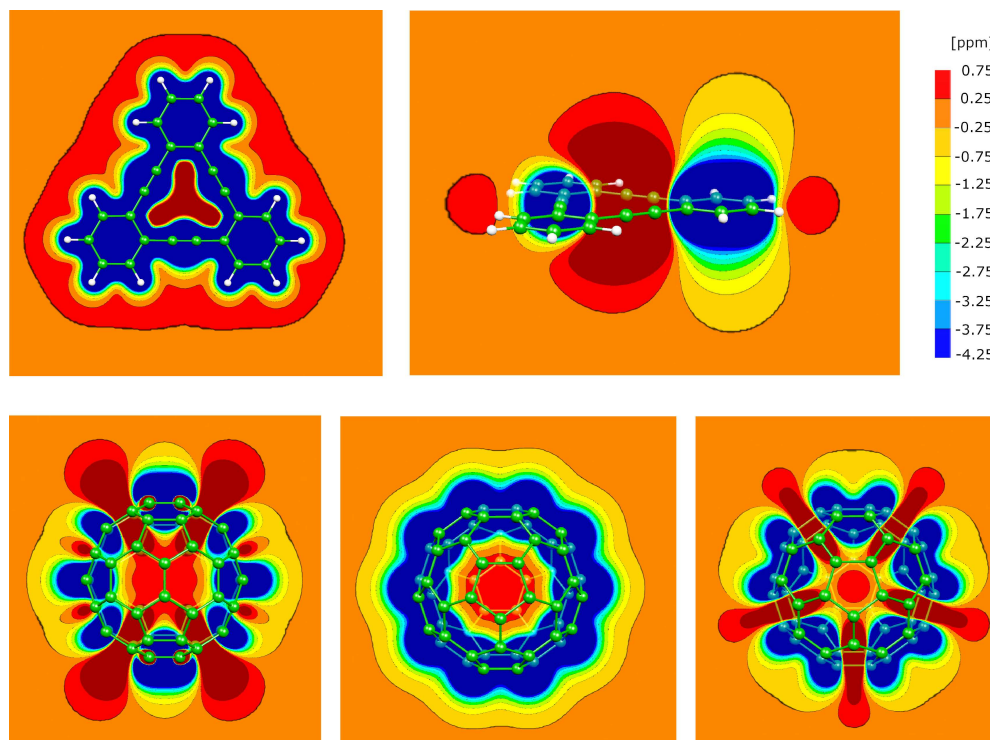
Table 2. Heats of formation of the different polyhedra (per carbon atom) considered in this work. The energy of the infinite graphene sheet (marked \star) has been taken as reference. Also reported are the number of pi-electrons in C_2 triple bonds (4 electrons per C_2), and the topology of the acetylene-connections between phenyl rings.

Polyhedron	Formation energy [kcal/mol per C]	Number of triple bonds	link topology
Graphyne sheet	0.0 \star		n/a ortho/meta/para
C_{60}	-4.31		n/a ortho/meta/para
PA trimer	0.10	3	ortho
PA hexamer	0.71	$6 = 2 \times 3$	para
PA decamer	0.86	$16 = 2 \times 2 \times 2 \times 2$	ortho/meta/para
P1	3.86	$6 = 2 \times 3$	meta
P2	1.56	$12 = 2 \times 2 \times 3$	meta
P4	0.47	$30 = 2 \times 3 \times 5$	meta
A1	1.12	$24 = 2 \times 2 \times 2 \times 3$	ortho/meta/para
A4	0.25	$60 = 2 \times 2 \times 3 \times 5$	ortho/meta/para

3.3. Cyclic phenylacetylene trimer and conventional Fullerene C_{60}

Figure 4 shows the NICS maps of the cyclic trimer of phenylacetylene (PA), first coplanar at a distance of about 1 Å from the molecular plane, and secondly at one of the mirror planes. As expected, the phenyl ring displays a strongly diatropic shielding cone, while the central triangular part of the molecule is deshielded (paratropic). The latter is a typical signature of an anti-aromatic electronic system. When considering the scale of the NICS field (shown in ppm), it turns out that the interplay of diatropic and paratropic fragments is approximately balanced. This situation is similar to the one found in one of the most common fullerenes, C_{60} , which is also shown in Figure 4. There, the five-membered rings have an anti-aromatic character, in “competition” with the aromatic six-membered rings. Altogether, the electronic subsystem yields a slight deshielding of the central part of the fullerene, although there are almost twice as many (aromatic) six-membered rings as five-membered ones. However, there is no overall dominance of either character, the shielded and deshielded regions vary depending on the location of the observation plane.

Figure 4. NICS maps of the phenylacetylene trimer (top) and the C₆₀ fullerene (bottom) in units of 10⁻⁶ (ppm). The same underlying data was used for the two (PA trimer) and three (C₆₀) slices, only the perspective (the orientation and position of the slice plane) is different.



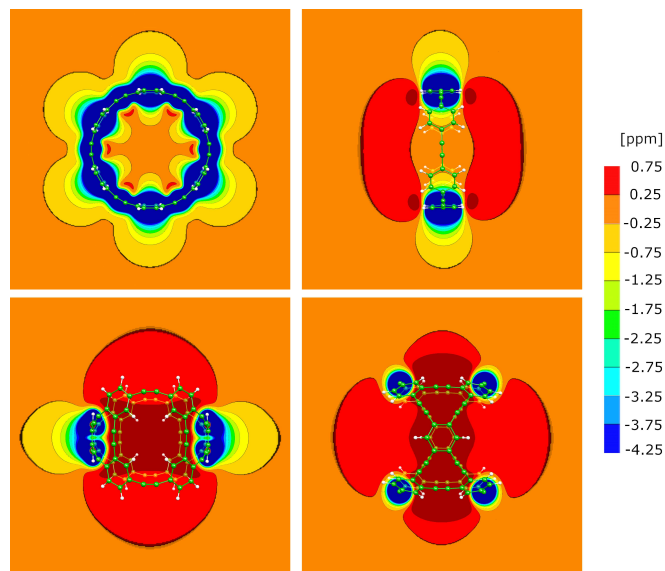
3.4. Necklace-style phenylacetylenes

We have further considered phenyl-acetylene molecules with a torus-like ring topology. The NICS maps of two such molecules, with six and ten PA building blocks, are shown in Figure 5. They exhibit a notably distinct picture: while in the hexamer, the shielding of the aromatic phenyl rings clearly dominates the overall character of the molecule, the decamer is mostly paratropic, especially in the center of the ring. Not only the center of the ring is deshielded, but also a significant region on the lateral sides of the supramolecular ring. This is surprising, as there are no less than ten phenyl rings whose shielding effect is superimposed in the center of the PA decamer.

In the PA hexamer, the phenylacetylenes are connected via the para positions of the phenyl rings, while in the case of the PA trimer (Figure 4), the acetylenes are attached on the ortho carbons. Both topologies are present in the decamer, where closed loops can be constructed on the basis of para- and ortho-connections, but also via the meta positions. In the meta- and para-connected cases, the loop contain four and six PA units, respectively (see the bottom left and right images in Figure 5).

Tentatively correlating these findings, it turns out that ortho-connected groups lead to a medium paratropic character (PA trimer), a para topology leads to a weak partially paratropic and partially diatropic response (PA hexamer), while the combination ortho/meta/para yields a relatively strong paratropic deshielding effect (PA decamer).

Figure 5. NICS maps of a PA hexamer (top) and a PA decamer (bottom), each from two different perspectives.

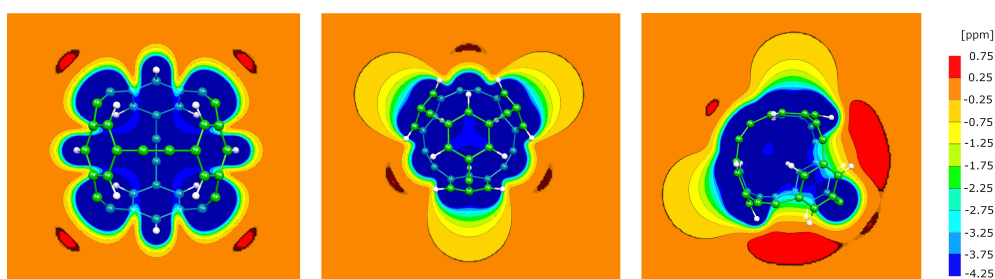


3.5. The P1 molecule

The smallest member of the P-series of phenylacetylenes is the P1 molecule, shown in Figure 6 with NICS maps at three different slice planes and molecular orientations. The overall character is strongly diatropic, with a shielding of about 5ppm inside the structure. There are almost no deshielded regions, the small red spots in Figure 6 are rather minor.

The connectivity between the PA groups is exclusively via meta carbons, which distinguishes P1 from the previously discussed molecules. As in the case of the PA trimer, the P1 molecule has (only) three-membered PA loops, but its magnetic response is strongly diatropic (as opposed to the paratropic signatures of the PA trimer, Figure 4). Thus, the presence of rings of three PA groups cannot be used as an explanation; however, the connection via meta-positions might be correlated to the magnetic response. While the PA decamer also exhibits this feature, their diatropic character could be compensated by the (more numerous) ortho-connected loops.

Figure 6. NICS maps of the P1 molecule.

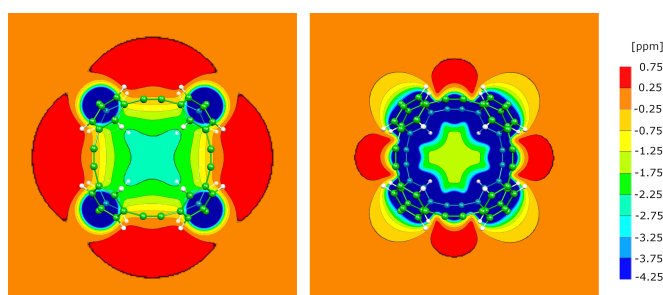


3.6. The P2 molecule

The P2 molecule and its NICS maps are shown in Figure 7. While the magnetic shielding at the center of the cage is noticeably smaller than that of P1, the diatropic signatures are still dominant. Nevertheless, there are larger paratropic areas, visible as a kind of red halo, which are a sign of a certain competition between the (aromatic) phenyl rings and the acetylene linkers.

As in the previous case (the P1 molecules), the covalent links between the PA groups in P2 are based only on the meta carbons of the phenyls. The difference to P1 is that the loops consist of four PA members instead of three, which does not affect the diatropic response of the molecule. The correlation between meta-connectivity and diatropic character, however, is confirmed.

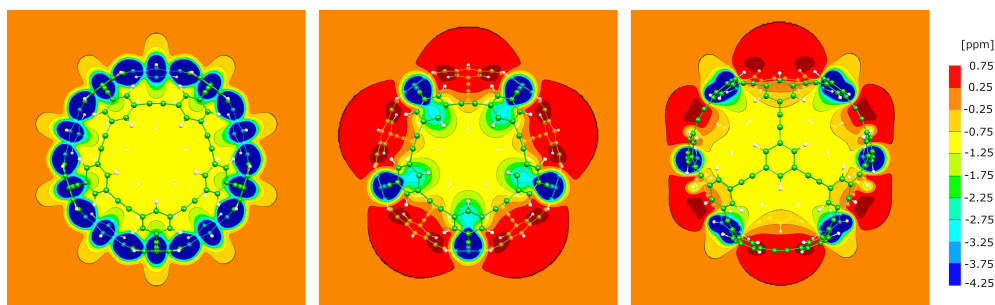
Figure 7. NICS maps of the P2 molecule.



3.7. The P4 molecule

The P4 molecule has an almost spherical shape and a magnetic response signature similar to the one of P2. Three NICS slices are presented in Figure 8, illustrating that the amplitude and size of the paratropic regions outside the molecule are larger than in the case of P1 and P2, while inside the cage, there is still a sizeable diatropic shielding of about one ppm.

Figure 8. NICS maps of the P4 molecule for three different slice planes.



Again, only meta positions are used to connect the PA units, which is again in line with the diatropic overall character of the molecule. In all closed loops in this molecule, the number of PA members per loop is five. Together with the corresponding values for P1 (three) and P2 (four), this makes an explicit

correlation between magnetic response and the number of triple bonds (*i.e.*, acetylene groups) per loop unlikely. Similarly, it seems not possible to related the total number of triple bonds in the entire molecule to the dia-/paratropic character. The weaker diatropic character compared to P1 and P2 can be explained with the considerably smaller number of PA groups per “surface area” of the molecular cage.

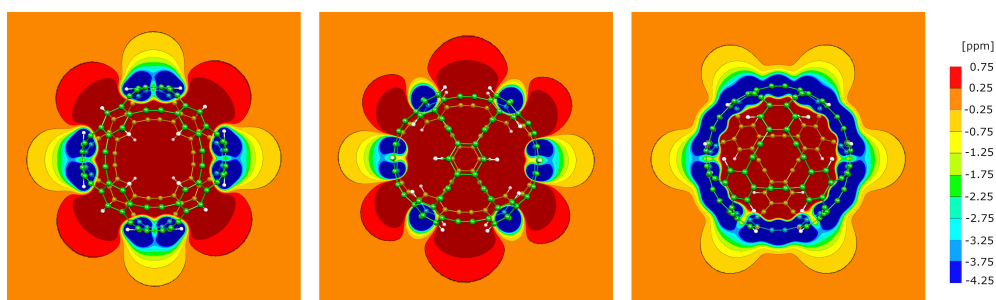
3.8. The A1 molecule

The second series of polyhedra has four acetylenes connected to each phenyl ring, and its smallest molecule (A1) is shown in Figure 9. While in the rightmost plot, the diatropic signatures of the aromatic phenyl rings towards the outside of the cage are still visible, the overall character of the system is strongly paratropic, with a considerable deshielding of +4.5 ppm in the center of the cage. This number is not directly visible in Figure 9 because it is outside the color coding range. It was extracted directly from the numerical shielding data.

This is to some degree surprising, since the difference in the electronic configuration with respect to P1/P2/P4 is not obvious. Notably, there are as many as ten phenyl rings (which are strongly aromatic), but they are not able to compensate the paratropic character of the remaining molecule. The NICS plots illustrate further that the triangular and the square-shaped faces contribute similar amplitudes to the paratropic character.

In A1, three-membered PA loops can be constructed via an ortho-connectivity, four-membered loops with meta-connections exist, and para-based loops with six PA members can also be found. In this respect, the situation is similar to the case of the PA decamer (Figure 5), where also all three connection types exist. Both the three-PA and four-PA loops exhibit paratropic signatures with an extended outreach: The red cones in Figure 9 have about the same size as the diatropic regions from the phenyl rings. Again, no correlation is obvious to the total number of triple bonds in the molecule.

Figure 9. NICS maps of the A1 molecule.



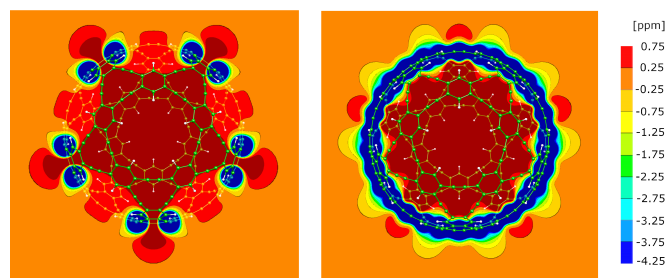
3.9. The A4 molecule

The biggest molecule in this study is the A4 one, which comprises 30 phenyl rings and 60 acetylene linkers. The NICS maps in Figure 10 show that the paratropic reaction dominates again. As in the case of A1, the center of the cage is strongly deshielded. However, the NICS amplitude in the cage (about +1 ppm) is considerably weaker than for the smaller A1. This trend has already been observed for the

P1/P2/P4 series of molecules, where the NICS shifts of the inner part of the molecular cages decreased (less diatropic character) when the molecule got bigger.

The three-PA and five-PA membered loops are again based on ortho- and meta-carbons, while the para-based loops have now ten PA members. This finding is in line with the previous results, which showed a strong paratropic response character in the case of mixed ortho/meta/para connectivities.

Figure 10. NICS maps of the A4 molecule.



4. Discussion and Conclusions

The diatropic and paratropic nucleus independent chemical shift maps of the considered polyhedral phenylacetylene molecules illustrate that it is not trivial to assign global “aromatic” and “anti-aromatic” characteristics to them. In many molecules, there are elements of both, and they partially compensate. This quasi-competition between dia- and paratropic regions shows that it is often not possible to quantify the concept of aromaticity with the help of a single number, *i.e.*, the nucleus independent chemical shift *value*. Instead, a visual representation of the corresponding three-dimensional maps can lead to the desired insight.

This magnetic response characteristics is not correlated to the number of π -electrons (via the number of triple bonds) per molecule or per closed loop, as in the analogous case of simple planar conjugated π -systems (the “ $4n + 2$ ”-rule). However, the type of connectivity between the phenyl groups plays an important role, resulting in different diatropic/paratropic signatures when the connectivity is realized using the meta-, ortho-, and para-positions, respectively. This is in line with the recent findings of Tobe *et al.* [14], who found strong aromatic signatures of 12-membered ring structures in planar oligo-graphynes.

It is noteworthy that the considerable curvature in the smaller molecules does not necessarily lead to a reduced magnetic shielding response. On the opposite, it is rather for the large molecules that a weakening of the intensity of dia- and paratropic characters is observed.

Acknowledgements

This work has been supported by the Deutsche Forschungsgemeinschaft (DFG) under grants SE 1008/5 and SE 1008/6.

References

1. Bacon, R. Growth, Structure, and Properties of Graphite Whiskers. *J. Appl. Phys.* **1960**, *31*, 283–290.
2. Kroto, H.W.; Heath, J.R.; O'Brien, S.C.; Curl, R.F.; Smalley, R.E. C-60 - Buckminsterfullerene. *Nature* **1985**, *318*, 162–163.
3. Grossman, J.C.; Cote, M.; Louie, S.G.; Cohen, M.L. Electronic and structural properties of molecular C-36. *Chem. Phys. Lett.* **1998**, *284*, 344–349.
4. Collins, P.G.; Grossman, J.C.; Cote, M.; Ishigami, M.; Piskoti, C.; Louie, S.G.; Cohen, M.L.; Zettl, A. Scanning tunneling spectroscopy of C-36. *Phys. Rev. Lett.* **1999**, *82*, 165–168.
5. Klimko, G.T.; Mestechkin, M.M.; Whyman, G.E.; Khmelevsky, S. C-28 and C-48 fullerenes special properties. *J. Mol. Struct.* **1999**, *481*, 329–333.
6. Romero, A.H.; Sebastiani, D.; Ramírez, R.; Kiwi, M. Is NMR the tool to characterize the structure of C₂₀ isomers? *Chem. Phys. Lett.* **2002**, *366*, 134–140.
7. Kroto, H.W. C-60 - Buckminsterfullerene, the Celestial Sphere That Fell To Earth. *Angew. Chem. Int. Ed.* **1992**, *31*, 111–129.
8. Prinzbach, H.; Weiler, A.; Landenberger, P.; Wahl, F.; Worth, J.; Scott, L.T.; Gelmont, M.; Olevano, D.; van Issendorff, B. Gas-phase production and photoelectron spectroscopy of the smallest fullerene, C₂₀. *Nature* **2000**, *407*, 60.
9. Piskoti, C.; Yarger, J.; Zettl, A. C-36, a new carbon solid. *Nature* **1998**, *393*, 771–774.
10. Weber, K.; Voss, T.; Heimbach, D.; Weiler, A.; Keller, M.; Worth, J.; Knothe, L.; Exner, K.; Prinzbach, H. From unsaturated dodecahedranes to C-40 cages? *Tetrahedron Lett.* **2005**, *46*, 5471–5474.
11. Wahl, F.; Weiler, A.; Landenberger, P.; Sackers, E.; Voss, T.; Haas, A.; Lieb, M.; Hunkler, D.; Worth, J.; Knothe, L.; Prinzbach, H. Towards perfunctionalized dodecahedranes - En route to C-20 fullerene. *Chem. Eur. J.* **2006**, *12*, 6255–6267.
12. Narita, N.; Nagai, S.; Suzuki, S.; Nakao, K. Optimized geometries and electronic structures of graphyne and its family. *Phys. Rev. B* **1998**, *58*, 11009–11014.
13. Kehoe, J.M.; Kiley, J.H.; English, J.J.; Johnson, C.A.; Petersen, R.C.; Haley, M.M. Carbon networks based on dehydrobenzoannulenes. 3. Synthesis of graphyne substructures. *Org. Lett.* **2000**, *2*, 969–972.
14. Tahara, K.; Yoshimura, T.; Sonoda, M.; Tobe, Y.; Williams, R.V. Theoretical studies on graphyne substructures: Geometry, aromaticity, and electronic properties of the multiply fused dehydrobenzo[12]annulenes. *J. Org. Chem.* **2007**, *72*, 1437–1442.
15. Jones, R.O.; Gunnarsson, O. The Density Functional Formalism, Its Applications and Prospects. *Rev. Mod. Phys.* **1989**, *61*, 689–746.
16. Hutter, J.; others. Computer code CPMD, version 3.12. Copyright IBM Corp. and MPI-FKF Stuttgart 1990-2008, www.cpmid.org.
17. Putrino, A.; Sebastiani, D.; Parrinello, M. Generalized Variational Density Functional Perturbation Theory. *J. Chem. Phys.* **2000**, *113*, 7102–7109.
18. Sebastiani, D.; Parrinello, M. A New Method to Compute NMR Chemical Shifts in Periodic

- Systems. *J. Phys. Chem. A* **2001**, *105*, 1951.
19. Sebastiani, D. Current Density Plots and Nucleus Independent Chemical Shift Maps (NICS) from Reciprocal Space Density Functional Perturbation Theory Calculations. *ChemPhysChem* **2006**, *7*, 164–175.
 20. Schleyer, P.v.R.; Maerker, C.; Dransfeld, A.; Jiao, H.; Hommes, N.J.R.v.E. Nucleus-Independent Chemical Shifts: A Simple and Efficient Aromaticity Probe. *J. Am. Chem. Soc.* **1996**, *118*, 6317–6318.
 21. Heine, T.; Schleyer, P.v.R.; Corminboeuf, C.; Seifert, G.; Reviakine, R.; Weber, J. Analysis of Aromatic Delocalization: Individual Molecular Orbital Contributions to Nucleus-Independent Chemical Shifts. *J. Phys. Chem. A* **2003**, *107*, 6470–6475.
 22. Moran, D.; Stahl, F.; Bettinger, H.F.; Schaefer, H.; Schleyer, P.v.R. Towards graphite: Magnetic properties of large polybenzenoid hydrocarbons. *J. Am. Chem. Soc.* **2003**, *125*, 6746–6752.
 23. Corminboeuf, C.; Heine, T.; Seifert, G.; Schleyer, P.v.R.; Weber, J. Induced magnetic fields in aromatic [n]-annulenes - interpretation of NICS tensor components. *Phys. Chem. Chem. Phys.* **2004**, *6*, 273–276.
 24. Sebastiani, D.; Kudin, K. Response Properties of Carbon Nanotubes in Magnetic Fields. *ACS Nano* **2008**, *2*, 661–668.
 25. Kirchner, B.; Sebastiani, D. Visualizing Degrees of Aromaticity. *J. Phys. Chem. A* **2004**, *108*, 11728–11732.
 26. Lazzeretti, P. Assessment of aromaticity via molecular response properties. *Phys. Chem. Chem. Phys.* **2004**, *6*, 217–223.
 27. Merino, G.; Heine, T.; Seifert, G. The induced magnetic field in cyclic molecules. *Chem. Eur. J.* **2004**, *10*, 4367–4371.
 28. Lazzeretti, P. Ring-Current Signatures in Shielding-Density Maps. *Chem. Phys. Lett.* **2005**, *401*, 164–169.
 29. Kleinpeter, E.; Fettke, A. Quantification of the (anti)aromaticity of fulvenes subject to ring size. *Tetrahedron Lett.* **2008**, *49*, 2776–2781.
 30. Gonze, X.; Vigneron, J.P. *Phys. Rev. B* **1989**, *39*, 13120.
 31. Gonze, X. *Phys. Rev. A* **1995**, *52*, 1096.
 32. Baroni, S.; de Gironcoli, S.; del Corso, A.; Giannozzi, P. Phonons and Related Crystal Properties from Density-Functional Perturbation Theory. *Rev. Mod. Phys.* **2001**, *73*, 515.
 33. Hohenberg, P.; Kohn, W. The Inhomogeneous Electron Gas. *Phys. Rev.* **1964**, *136*, B864.
 34. Kohn, W.; Sham, L.J. Self-Consistent Equations Including Exchange and Correlation Effects. *Phys. Rev.* **1965**, *140*, A1133.
 35. Goedecker, S.; Teter, M.; Hutter, J. Separable Dual-Space Gaussian Pseudopotentials. *Phys. Rev. B* **1996**, *54*, 1703.
 36. Hartwigsen, C.; Goedecker, S.; Hutter, J. Relativistic Separable Dual-Space Gaussian Pseudopotentials from H to Rn. *Phys. Rev. B* **1998**, *58*, 3641.
 37. Becke, A.D. Density-Functional Exchange-Energy Approximation With Correct Asymptotic Behavior. *Phys. Rev. A* **1988**, *38*, 3098.
 38. Lee, C.; Yang, W.; Parr, R.G. Development of the Colle-Salvetti Correlation-Energy Formula into

- a Functional of the Electron-Density. *Phys. Rev. B* **1988**, *37*, 785–789.
39. Johnson, C.E.; Bovey, F.A. Calculation of Nuclear Magnetic Resonance Spectra of Aromatic Hydrocarbons. *J. Chem. Phys.* **1958**, *29*, 1012–1014.
 40. Aihara, J.I. Nucleus-independent chemical shifts and local aromaticities in large polycyclic aromatic hydrocarbons. *Chem. Phys. Lett.* **2002**, *365*, 34–39.
 41. Steiner, E.; Fowler, P.W.; Jenneskens, L.W.; Havenith, R.W.A. Local and global paratropic and diatropic ring currents in pyrene and its cyclopenta-fused congeners. *Eur. J. Org. Chem.* **2002**, *365*, 163–169.
 42. Matsuo, Y.; Tahara, K.; Nakamura, E. Theoretical Studies on Structures and Aromaticity of Finite-Length Armchair Carbon Nanotubes. *Org. Lett.* **2003**, *5*, 3181–3184.
 43. Poater, J.; Fradera, X.; Duran, M.; Sola, M. An Insight into the Local Aromaticities of Polycyclic Aromatic Hydrocarbons and Fullerenes. *Chem. Eur. J.* **2003**, *9*, 1113–1122.
 44. Fowler, P.W.; Soncini, A. Aromaticity, polarisability and ring current. *Chem. Phys. Lett.* **2004**, *383*, 507–511.
 45. Fowler, P.W.; Steiner, E.; Havenith, R.W.A.; Jenneskens, L.W. Current Density, Chemical Shifts and Aromaticity. *Magn. Reson. Chem.* **2004**, *42*, S68–S78.

© 2009 by the authors; licensee Molecular Diversity Preservation International, Basel, Switzerland. This article is an open-access article distributed under the terms and conditions of the Creative Commons Attribution license <http://creativecommons.org/licenses/by/3.0/>.